THE JOURNAL OF PHYSICAL CHEMISTRY C

Article

pubs.acs.org/JPCC

Anisotropic Seeded Growth of Cu–M (M = Au, Pt, or Pd) Bimetallic Nanorods with Tunable Optical and Catalytic Properties

Shutang Chen,[†] Samir V. Jenkins,[†] Jing Tao,[‡] Yimei Zhu,[‡] and Jingyi Chen*,[†]

[†]Department of Chemistry and Biochemistry, University of Arkansas, Fayetteville, Arkansas 72701, United States

[‡]Condensed Matter Physics and Materials Science Department, Brookhaven National Laboratory, Upton, New York 11973, United States

Supporting Information

ABSTRACT: A general strategy to synthesize Cu–M (M = Au, Pt, or Pd) bimetallic nanorods has been demonstrated based on a seeded co-reduction method. In this approach, noble metal nanoparticles serve as seeds, and newly reduced Cu atoms are subsequently nucleated on one side of the seeds, resulting in Janus nanoparticles with an M-rich and a Cu-rich portion. The elongation of the particles originates from the site-specific deposition of Cu clusters on the Cu-rich side of these Janus nanoparticles by retarding reduction kinetics of Cu through galvanic replacement. Using this approach, Cu–M alloyed nanorods can be conveniently synthesized with tunable composition, crystal structure, and aspect ratio. These nanorods have also been demonstrated as a unique system for investigation of the structural and compositional effects on their optical and catalytic properties.

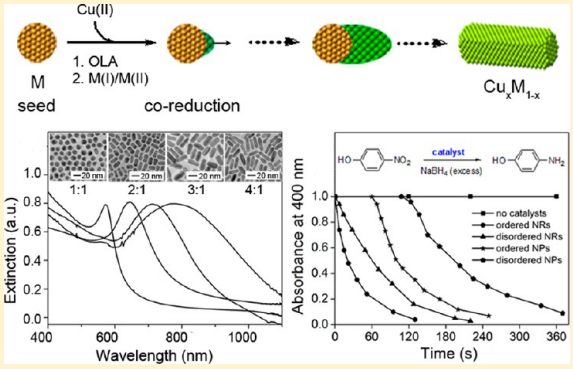

INTRODUCTION

Bimetallic nanostructures are emerging as a new class of attractive advanced materials with bifunctionality and enhanced catalytic properties as compared to their individual components.[1−3] According to their atomic arrangement, they are generally classified into three categories: core–shell structures, heterostructures, and mixed structures (i.e., alloy or intermetallic). Morphological control of bimetallic nanoparticles is of great interest because their properties are strongly correlated with their size and shape in addition to composition. In the past decade, much progress has been made in the chemical synthesis of bimetallic nanoparticles with well-defined morphology using different solution-based synthetic methods, such as co-reduction, thermal decomposition, galvanic replacement, and seeded growth.[3] Among them, the seeded growth method is particularly attractive for the controlled synthesis of core–shell structures or heterostructures. This method was originated by Murphy[4] and El-Sayed[5] and first introduced by Yang and co-workers as a robust method for shape-controlled synthesis of bimetallic nanostructures.[6] Since then, it has been applied to generate a variety of functional bimetallic nanostructures such as Ag–Au–Ag segmented nanorods,[7] Pd–Pt and Pd–Rh nanodendrites,[8−10] Pd–Au core–shell and dimer structures,[11−13] Pt–Au heterostructures,[14] and Au–Pd concave, convex, and other structures containing high-index planes.[15−17] More recently, this method has been combined with co-reduction as a new route for preparation of more complex Au–Pd bimetallic nanostructures.[18−20] In contrast to noble metals, the progress of seeded methods for bimetallic nanoparticles containing a 3d transition metal and a noble metal is rather limited due to the large difference of redox potentials.[21] In this case, the noble metal served as the seed, and its morphology was adapted to form core–shell or alloyed nanostructures depending on the miscibility of the two solid phases and the reaction temperature.[22−25] In this work, we report an anisotropic seeded growth of Cu-based bimetallic nanorods in which an inhomogeneous nucleation is introduced by controlling the reduction kinetics, thereby guiding the growth of nanocrystals in one direction and forming alloyed nanorods.

Copper nanostructures possess unique electronic, optical, and catalytic properties suitable for applications ranging from electronics[26,27] to photonics[28−30] and heterogeneous catalysis.[2,31,32] Alloying Cu with a noble metal has attracted considerable attention because of the synergistic effect of the binary system. For example, the localized surface plasmon resonance (LSPR) profile (i.e., position and width) varies with the Cu content in the alloyed nanoparticles, which is hard to predict theoretically using the dielectric constant calculated by the simple linear mixing rule.[33,34] The catalytic performance of Cu–Au nanoparticles outperformed their individual components for oxidation of CO, benzyl alcohol, and propene,[2] as well as reduction of CO_2.[35] The catalytic reactivity and selectivity depend on the crystal structure (disordered vs ordered) and the shape (e.g., solid vs porous) of nanoparticles aside from the composition. In recent years, considerable knowledge has been contributed to the synthesis of these Cu-containing binary

Received: February 6, 2013
Revised: April 5, 2013
Published: April 9, 2013

   dx.doi.org/10.1021/jp4013653 | J. Phys. Chem. C 2013, 117, 8924–8932

systems. Schaak and co-workers demonstrated a solution method to prepare Cu−Au alloyed and intermetallic nanoparticles by directly alloying the Cu and Au nanoparticle precursors or co-reducing their salt precursors at much lower than traditional metallurgical temperatures.[36,37] Recently, Li and co-workers reported a seeded-based diffusion route by reducing Cu salt precursors in the presence of Au seeds to synthesize intermetallic Cu−Au nanoparticles with uniform size.[23] Henkel et al. prepared alloyed nanorods of Cu−Au by co-reducing Cu and Au using a modified synthesis of Au nanorods.[33] For other Cu-based alloys, the co-reduction method was optimized to obtain Pt−Cu nanorods[38] and nanocubes,[39] as well as Pd−Cu nanocubes and tetrapods,[40] using various combinations of surfactants in the synthesis. Despite these advancements, the morphological control of these bimetallic nanostructures remains to be challenging, and the underlying mechanism is still lacking. In this paper, we have developed a seeded co-reduction method using a two-step procedure in a simple system involving only aliphatic amine and metal salt precursors in the reaction. One-dimensional (1D) growth was induced by controlling the reduction kinetics of the secondary metal, resulting in the asymmetric nucleation on the noble metal seeds. Using this method, we have demonstrated that the Cu−M (M = Au, Pt, and Pd) alloyed nanorods could be synthesized with controllable composition and aspect ratio. At elevated temperature, these alloyed nanorods with a disordered face-centered-cubic (fcc) structure could be transformed to intermetallic nanorods with atomically ordered structure. The optical and catalytic properties of these nanostructures have been found to be governed by the compositional, structural, and morphological variables.

EXPERIMENTAL SECTION

Chemicals. Copper 2,4-pentanedionate ($Cu(acac)_2$, 98%), copper chloride ($CuCl_2$), copper acetate ($Cu(CH_3COO)_2$), hydrogen tetrachloroaurate trihydrate ($HAuCl_4{\cdot}3H_2O$), octadecylamine (ODA, 98%), dodecylamine (DDA, 98%), *p*-nitrophenol, silver nitrate ($AgNO_3$), platinum 2,4-pentanedionate ($Pt(acac)_2$), palladium 2,4-pentanedionate ($Pd(acac)_2$), and sodium borohydride ($NaBH_4$) were purchased from Alfa Aesar. Oleylamine (OLA, 80−90%) was purchased from Acros. Tetradecylamine (TDA, 98%) was purchased from TCI. Oleylamine (OLA, 70%), hexadecylamine (HDA, 98%), and methoxypoly(ethylene glycol) amine ($PEG\text{-}NH_2$) (MW = 5000) were purchased from Sigma-Aldrich. All chemicals were used as received unless specified otherwise.

Synthesis of Cu−M Bimetallic Nanorods. In a typical synthesis, OLA (20 mmol) and $HAuCl_4{\cdot}3H_2O$ (0.05 mmol, 19.7 mg) were added to a 25 mL three-neck flask equipped with a magnetic stir bar. For DDA, TDA, HDA, or ODA, equimolar amounts of amine were used to replace OLA. Argon was blown over the reaction mixture for 10 min to remove O_2. The reaction mixture was heated to 160 °C, and the color of the solution mixture changed from yellow (50−65 °C) to colorless (65−115 °C), pale pink, and ruby red (115−120 °C), indicating that the Au(III) was reduced to Au(I) and then Au(0). The reaction was kept at 160 °C for 20 min and then cooled to 60 °C. Without separation, $Cu(acac)_2$ (52.4 mg, 0.2 mmol) in 1 mL of OLA was then injected to the reaction mixture, followed by heating to 180 °C, which was maintained for another 20 min. For $CuCl_2$ or $Cu(CH_3COO)_2$, equal amounts of Cu precursor in 1 mL of OLA were used to replace $Cu(acac)_2$. For synthesis of Cu_3Au intermetallic nanorods, the reaction mixture was further heated to 280 °C and kept at this temperature for another 20 min. After the reaction, the product was purified by adding toluene and centrifuging at 3300 rpm for 2 min to remove excess reactants and surfactants.

To control the aspect ratio of the nanorods, the concentration of $HAuCl_4{\cdot}3H_2O$ was varied while the mole ratio of Au and Cu precursors was kept at 1:4. When the concentration of $HAuCl_4{\cdot}3H_2O$ was reduced from 0.05 to 0.02, 0.01, and 0.005 M, the aspect ratio of the Cu_3Au nanorods was increased from 1:1 to 2:1, 3:1, and 4:1 under the same reaction conditions as described previously.

To control the composition, the mole ratio of Au and Cu precursors was reduced from 1:4 to 1:2 for CuAu nanorod synthesis, while the Au precursors were replaced by $Pt(acac)_2$ and $Pd(acac)_2$ for Cu_3Pt and Cu_3Pd nanorod syntheses, respectively.

Phase Transfer of Cu_3Au Nanostructures from Organic Phase to Aqueous Phase. $PEG\text{-}NH_2$ (2.0 μmol, 10 mg) was dissolved in 15 mL of $CHCl_3$ in a 25 mL flask. After stirring for ∼10 min in an ice bath, Cu_3Au nanostructures (5−6 mg) in 2.0 mL of toluene were added dropwise to the solution. The reaction solution was degassed with argon for 5 min and allowed to stir overnight in the dark. After that, the PEGylated nanostructures were purified by first precipitating with hexane and sequentially washing by ethanol and water. The products were finally dispersed in 2 mL of deionized water for the catalytic studies.

Catalytic Studies. In a typical measurement, aqueous solutions of *p*-nitrophenol (1.4 mM) and $NaBH_4$ (0.42 M) were freshly prepared as separate stock solutions. Deionized water (7.0 mL) was mixed with 0.5 mL of *p*-nitrophenol stock solution. The color of the solution changed from colorless to yellow as soon as 1.0 mL of $NaBH_4$ stock solution was added. Then, 0.2 mL of PEGylated Cu_3Au nanorod catalysts was added into the system with a final concentration of 2.5×10^{10} rods/mL. Immediately after mixing, 2.0 mL of the reaction solution was quickly transferred into a quartz cuvette, and the absorbance spectra were recorded using UV−vis spectrometer over a certain period of time. The nanorods have roughly the same dimensions (26.7 × 9.5 nm), and the total surface area for nanorods in each solution is 2.2×10^{13} nm^2/mL. To keep the concentration of Au atoms (8.38×10^{-8} mol/mL) roughly on the same scale for all catalysts, 0.5 mL of the nanoparticle catalysts was used with a final concentration of 3×10^{11} particles/mL. The nanoparticles have roughly the same diameter (9.5 nm), and the total surface area for nanorods in each solution is 8.5×10^{13} nm^2/mL.

Instrumentation. Transmission electron microscopy (TEM) images were captured using a JEOL 100cx microscope with an accelerating voltage of 100 kV. High angle annular dark field scanning transmission electron microscopy (HAADF-STEM) images, high-resolution TEM (HRTEM) images, and energy-dispersive X-ray (EDX) mapping were obtained using a JEOL 2100F microscope with an acceleration voltage of 200 kV, equipped with heating and cooling *in situ* TEM sample holder. X-ray diffraction (XRD) patterns were acquired using a Rigaku MiniFlex X-ray diffractometer equipped with Cu Kα radiation source operated at 30 kV/15 mA. The concentrations of Au and Cu were determined using a GBC 932 atomic absorption (AA) spectrometer. UV−vis spectra were taken on an HP 8453 UV−vis spectrophotometer.

dx.doi.org/10.1021/jp4013653 | J. Phys. Chem. C 2013, 117, 8924−8932

RESULTS AND DISCUSSION

Figure 1 illustrates the evolution of noble metal seeds (M = Au, Pt, or Pd) to Cu_xM_{1-x} nanorods using a two-step procedure

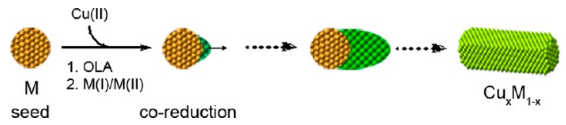

Figure 1. Schematic illustration of the seeded co-reduction strategy for the synthesis of bimetallic Cu-based nanorods in which noble metal (M) seeds were formed *in situ*, followed by co-reducing Cu and M precursors in the second step. The 1D growth was driven by asymmetrically depositing Cu on the M seeds, and the diffusion led to the formation of alloy.

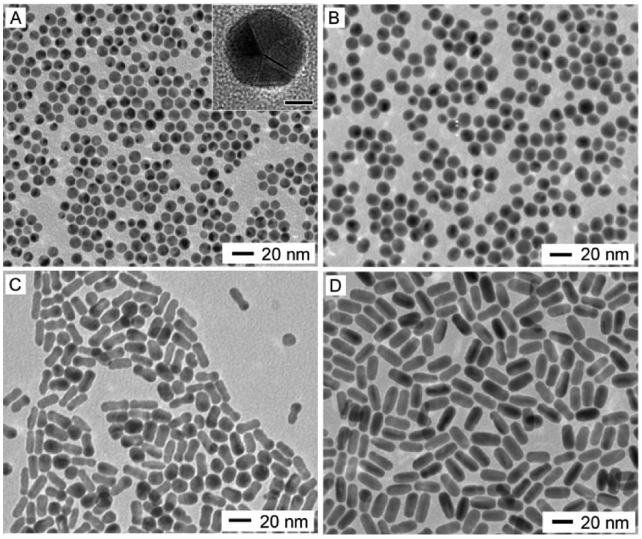

Figure 2. TEM images of the particles in aliquots collected from a seeded co-reduction synthesis of Cu_3Au nanorods at different time points: (A) the Au seeds formed *in situ* and (B–D) 1, 5, and 20 min after the Cu precursors had been added into the reaction mixture, respectively. The inset of (A) shows HRTEM of an individual Au seed.

involving seed-mediated co-reduction in aliphatic amine, such as $C_nH_{2n+1}NH_2$, $n \geq 12$, or oleylamine (OLA). In this method, the amine serves as a coordinating ligand, reducing agent, capping ligand, and solvent.[23,41,42] Initially noble metal nanoparticles were formed as seeds by reducing their amine complex, M(I) or M(II), in the absence of Cu precursors. After Cu precursor, Cu(II), was injected into the reaction mixture, they were reduced to Cu^0 by the amine and subsequently nucleated on the surface of the seeds. The Cu(II) could be adsorbed and reduced on the seed surface,[24] or it could be reduced in solution before nucleation on the seed surface.[43] To introduce anisotropic growth, it is essential to convert isotropic seeds to Janus nanoparticle intermediates containing an M-rich and a Cu-rich side. This anisotropy can be achieved by controlling the reduction kinetics of Cu. Relatively slow reduction kinetics should be maintained to avoid uniform nucleation of Cu around each seed;[44−46] however, the reduction of Cu needs to overwhelm the galvanic replacement between M(I)/M(II) and Cu^0 as well as the diffusion between M and Cu. Once the Janus nanoparticles form, the newly formed Cu^0 can then preferentially deposit on the Cu-rich side because of the large lattice mismatch between Cu (a = 3.61 Å) and M (a = 4.07, 3.92, and 3.89 Å for Au, Pt, and Pd,

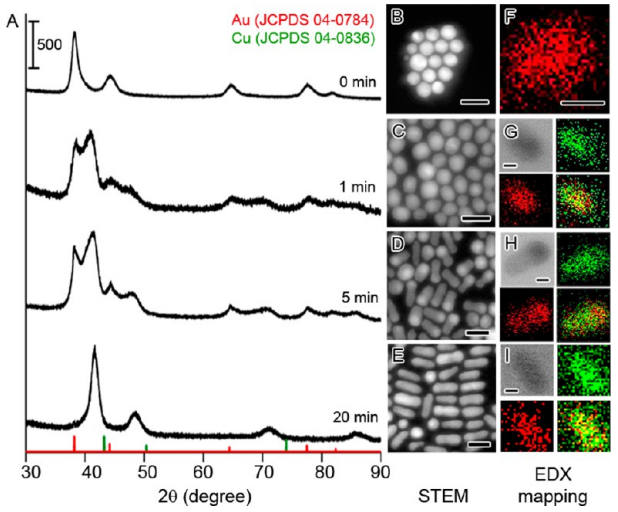

Figure 3. Structural characterization of the aliquot samples corresponding to the samples in Figure 2: (A) XRD and (B–E) HAADF-STEM. (F) EDX mapping of Au element in the seed sample in (B). (G–I) EDX mapping of samples in (C, D) with four panels: bright-field image, mapping of Cu (green), mapping of Au (red), and their overlaid image. The scale bars in the HAADF-STEM images are 20 nm while the scale bars in the bright-field images of EDX mapping are 5 nm.

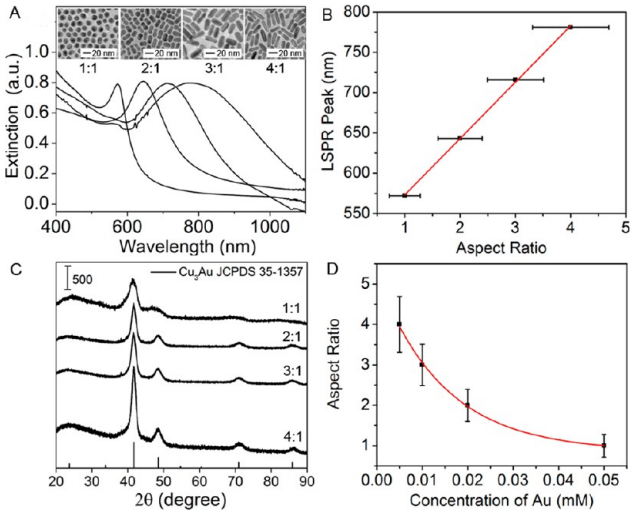

Figure 4. (A) UV–vis–NIR spectra of Cu_3Au nanorods with LSPR peaks at 572, 643, 716, and 781 nm as aspect ratio increases from 1:1 to 4:1. The insets are the corresponding TEM images. (B) Plot of the LSPR peak as a function of aspect ratio of the Cu_3Au nanorods. The red line is the linear fit of the solid-square experimental data (y = 503 + 70x; R = 0.999). (C) XRD characterization of the Cu_3Au nanorods corresponding to the samples in (A), suggesting that all of them possess a disordered fcc phase. (D) Plot of aspect ratio of the Cu_3Au nanorods as a function of the Au precursor concentration (mole ratio Au:Cu = 1:4). The red line is the exponential fit of the solid-square experimental data ($y = 0.88 + 4.39e^{-70.36x}$; R = 0.997). The error bars of the aspect ratios are propagated from the uncertainties of length and width of the nanorods.

respectively). As a result, growth was driven in one direction, forming rod-shaped nanoparticles. During the thermal annealing process, the atoms gradually diffuse from one position to another within the nanorods, resulting in a mixed alloy composition that adopts a disordered fcc structure.

dx.doi.org/10.1021/jp4013653 | J. Phys. Chem. C 2013, 117, 8924−8932

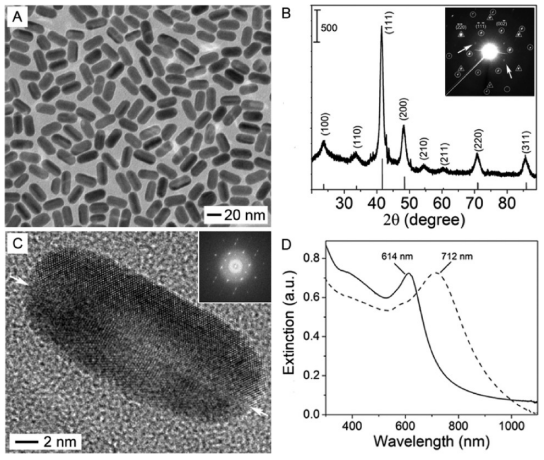

Figure 5. (A) TEM image of the ordered cubic Cu_3Au nanorods prepared by thermally annealing the disordered sample in solution phase. (B) XRD pattern of the sample shown in (A), indicating an ordered cubic Cu_3Au phase. The black lines correspond to the standard pattern of the ordered cubic Cu_3Au phase (JCPDS 35-1357). The inset is the ED pattern of an individual Cu_3Au nanorod. The spots labeled in circles were observed from the [110] zone, and those labeled in triangles were viewed down the [111] zone axis. The arrows indicate the (110) reflections, suggesting an ordered cubic Cu_3Au phase. (C) HRTEM of an individual Cu_3Au nanorod. The inset shows a FFT pattern of the HRTEM. The interface between two single-crystal domains was indicated by the arrows. (D) UV−vis−NIR spectra of the Cu_3Au nanorods before (dashed line) and after (solid line) heat treatment at 280 °C in solution phase for 20 min.

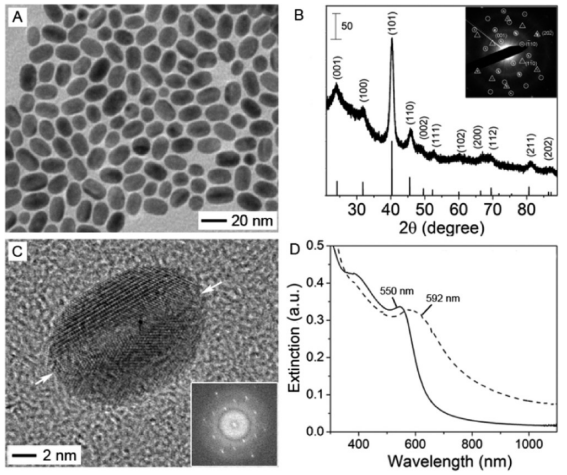

Figure 7. (A) TEM image of the intermetallic CuAu nanorods with dimensions of 17.7 ± 4.2 × 9.9 ± 1.9 nm. (B) XRD pattern of the sample shown in (A), indicating an ordered tetragonal CuAu phase. The black lines correspond to the standard pattern of the ordered tetragonal CuAu phase (JCPDS 65-2798). The inset is the ED pattern of an individual CuAu nanorod. The spots labeled in circles were observed from the [110] zone, and those labeled in triangles were viewed down the [111] zone axis. (C) HRTEM of an individual CuAu nanorod. The inset shows a FFT pattern of the HRTEM. The interface between two single-crystal domains is indicated by the arrows. (D) UV−vis spectra of the CuAu nanorods before (dashed line) and after (solid line) heat treatment at 280 °C in solution phase for 20 min.

This approach was initially demonstrated in the Cu−Au system to generate Cu_3Au alloyed nanorods. In a typical synthesis, the Au precursor was partially reduced to generate the initial seeds before addition of a Cu precursor. The color of the reaction mixture changed from golden yellow to colorless and then pink, indicating the formation of Au(I) amine complexes together with Au nanoparticles. Without purification, a Cu precursor was introduced into the reaction mixture in the form of Cu(II) amine complexes. The mechanism was elucidated by examining aliquots taken from the reaction mixture at different time points. The Au seeds, which were formed after the reaction had proceeded at 160 °C for 20 min, were multiply twinned nanoparticles bounded by {111} facets with a diameter less than 10 nm (Figure 2A). After the addition of Cu(II) amine complexes, the reaction temperature was raised to 180 °C to facilitate the reduction. One minute later, most of the seeds were found to be elongated, and they grew further along one direction until t = 5 min (Figure 2B,C). At t = 20 min, the elongated nanoparticles had transformed into nanorods with dimensions of 25.2 ± 1.5 × 8.5 ± 1.2 nm (Figure 2D). To validate the seeded co-reduction process, the reaction was decoupled into two successive steps while keeping the same reaction conditions.[18,19] The Au seeds were isolated and purified to remove the excess Au precursors at the end of the first step with a yield of ∼50%. Subsequently, these seeds

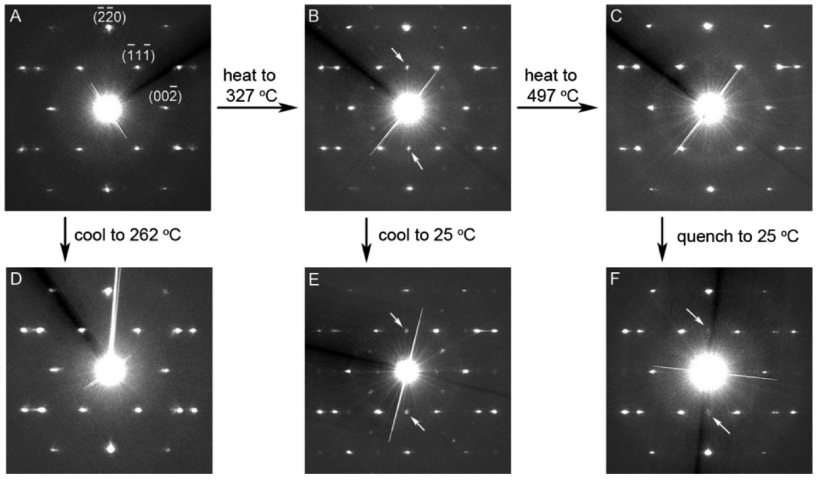

Figure 6. Phase transitions of Cu_3Au nanorods as a function of temperature by monitoring the appearance and disappearance of (110) reflection spots (as indicated by white arrows) in the ED patterns from individual nanorods.

dx.doi.org/10.1021/jp4013653 | J. Phys. Chem. C 2013, 117, 8924−8932

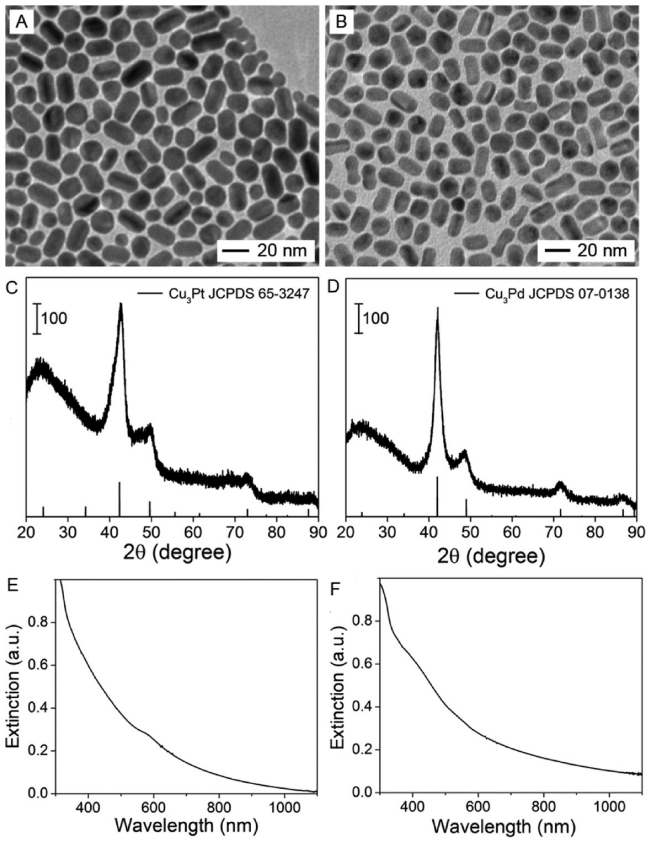

Figure 8. TEM of Cu-based bimetallic nanorods: (A) Cu_3Pt and (B) Cu_3Pd. (C, D) XRD characterization of corresponding samples in (A) and (B), respectively, indicating both of them are disordered alloys. (E, F) UV−vis spectra of corresponding samples in (A) and (B), respectively.

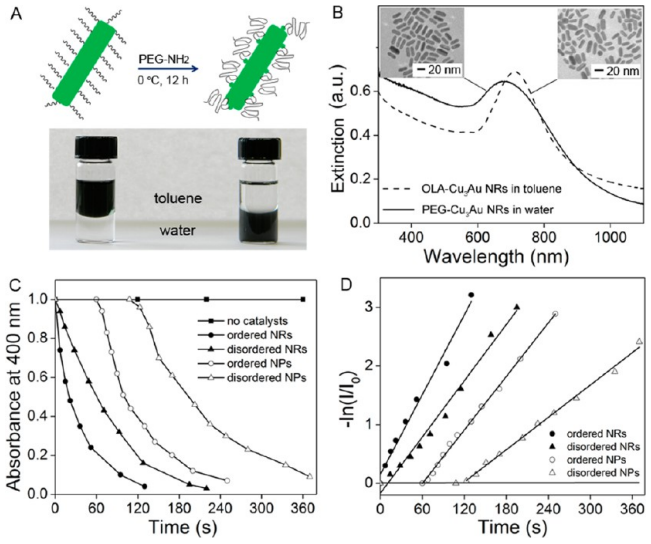

Figure 9. (A) Schematic illustration of the phase transfer of Cu_3Au nanostructures from organic phase to aqueous phase with the nanorods as an example. The photograph shows the Cu_3Au nanorod dispersion before and after phase transfer. (B) UV−vis−NIR spectra of Cu_3Au dispersion before (in toluene) and after phase transfer (in water) with LSPR peak at 716 and 684 nm, respectively. The inset shows their corresponding TEM images with 20 nm scale bar. (C) Plot of normalized absorbance (I/I_0) of *p*-nitrophenolate ion at 400 nm as a function of time for different catalysts. (D) Plot of $-\ln(I/I_0)$ as a function of time for different catalysts. The solid lines are the linear fit of the data and the slope gives k_{app} of the reaction.

were redispersed in OLA and heated to 60 °C. The Cu and Au precursors (8:1 ratio) were simultaneously added to the reaction mixture and co-reduced to yield Cu_3Au nanorods (Figure S1A,C). In the control experiment, when only Cu precursor was added to the mixture in the second step, Au/$CuAu_3$@Cu core−shell nanoparticles were found as final products (Figure S1B,D). Note that the Cu shell was quickly oxidized to CuO in air.

The structures of each sample obtained at different stages of a synthesis were analyzed by XRD (Figure 3A). The mole fraction of Cu and Au in the alloys was analyzed using Vegard's law, which holds a linear relation between the crystal lattice parameter (a) of an alloy and the mole fraction of the constituent elements (x).[47] During the synthesis, the pure fcc Au phase (a = 4.07 Å) at t = 0 min evolved to the single-phase disordered fcc Cu_3Au alloy (a = 3.75 Å) at t = 20 min. The intermediates at t = 5 or 10 min were indexed as mixtures of Au-rich and Cu-rich solid solutions with multiple fcc phases, as indicated by the broadened XRD patterns with an a value between those of Au and Cu. The reaction process was also monitored by UV−vis spectra with the LSPR maximum gradually shifting from 524 nm to 562 and 681 nm (Figure S2).

To reveal the morphology and composition of individual nanostructures, aliquots from a synthesis were further examined using HAADF-STEM, as shown in Figure 3B−E. Because the thickness of the sample is almost uniform along the entire nanorod, the HAADF-STEM images can be interpreted based on mass contrast with the Au-rich area brighter than the Cu-rich portion. Together with the compositional mapping by EDX (Figure 3F−I), the structural evolution during the synthesis is evident that the initial Au seeds become Janus structures with one side rich in Au and the other rich in Cu and then grow to alloyed nanorods. Note that the contrast variation for different particles in the HAADF-STEM images (Figure 3B,E) could be attributed to the diffraction contrast, resulting from the different crystal orientation of the particles. In the nanometer regime, the diffusion between Cu and Au is rapid and spontaneous with diffusivities on the same order of magnitude.[48,49] The diffusion process could be further accelerated by increasing the temperature.[50,51] An extension of the reaction time at an elevated temperature assisted the diffusion between Au and Cu within the nanoparticle, resulting in a homogeneous distribution of each element across the entire particle. Further analysis of the HAADF-STEM image of sample in Figure 3D at a relatively low magnification showed that one end of individual particles contains more Au compared to the entire particle (Figure S3). We concluded that the formation of nanorods were the result of heterogeneous nucleation as described in Figure 1. Although we could not rule out the possibility that the nanorods might result from the particle coalescence,[36,52] it is unlikely to occur in this case.

The aspect ratios of the Cu_3Au nanorods could be tuned by varying the precursor concentrations while keeping their mole ratio constant. Adjusting only the concentration allowed the aspect ratio to be tuned without affecting the final composition. A decrease in Au precursor concentration led to decreases in both size and concentration of the Au seeds and thus an increase in aspect ratio for the resultant nanorods. A mole ratio of 1:4 for the Au and Cu precursors yielded nanorods with a Au:Cu ratio of 1:3. The aspect ratio of Cu_3Au nanorods increased from 1:1 (12.7 ± 2.5 nm) to 2:1 (18.0 ± 2.6 × 8.9 ±

dx.doi.org/10.1021/jp4013653 | J. Phys. Chem. C 2013, 117, 8924−8932

Table 1. List of the Apparent Rate Constants (k_{app}) and Introduction Periods (t_0) of Different Catalysts for the Reduction of *p*-Nitrophenol at Room Temperature

catalyst	ordered NRs	disordered NRs	ordered NPs	disordered NPs
k_{app} (s^{-1})	0.0231 ± 0.0017	0.0160 ± 0.0050	0.0152 ± 0.0025	0.0091 ± 0.0025
t_0 (s)	0	0	59.4 ± 7.2	108.0 ± 52.2

1.2 nm), 3:1 (28.8 ± 2.3 × 10.6 ± 1.6 nm), and 4:1 (33.7 ± 4.4 × 8.1 ± 0.9 nm) with decreasing concentration of Au precursor (Figure 4A). The LSPR peak of the Cu_3Au nanorods was shifted linearly toward longer wavelength from 572 to 643, 716, and 781 nm with increased aspect ratios (Figure 4B). The Cu_3Au fcc phase of each sample was confirmed by XRD analysis (Figure 4C). Surprisingly, it was found that the plot of aspect ratio (y) as a function of concentration (x) could be well fitted by an exponential decay, $y = 0.88 + 4.39e^{-70.36x}$ (Figure 4D). Mathematically, a maximum aspect ratio is found at 5.28:1 ($y \rightarrow 5.28$) as the concentration of Au precursor approaches 0 ($x \rightarrow 0$). In practice, it is hard to increase the aspect ratio of nanorods beyond 4:1 by further lowering the precursor concentration under these experimental conditions because no nucleation occurs at extremely low concentration of reduced atoms.[53]

The disordered fcc phase was converted to ordered intermetallic phase by further annealing the alloyed Cu_3Au nanorods at 280 °C in solution. This disorder−order transition temperature is similar to that observed in the previous study.[36] Figure 5A−C shows structural characterization of the atomically ordered Cu_3Au nanorods with dimensions of 26.9 ± 3.0 × 12.7 ± 1.4 nm. The XRD pattern clearly shows the sharp peaks of superlattice (100) and (110) reflections, suggesting an ordered cubic Cu_3Au phase, where the Cu atoms are at the face centers and Au atoms occupy the corners in one unit cell, with a = 3.77 Å ($a_{lit.}$ = 3.75 Å).[54] The electron diffraction (ED) pattern from an individual nanorod in the inset showed two sets of spots viewed along the [111] and [110] zones, respectively. The spots of (110) reflections, which are forbidden from disordered fcc Cu_3Au alloy, were clearly observed on the ED pattern (as marked by the arrows) of an ordered phase. The analysis of ED and fast Fourier transform (FFT) of the HRTEM suggested that the atomically ordered cubic Cu_3Au nanorod grew along ⟨110⟩ direction, with two single-crystal domains being assembled along the longitudinal axis. During the disorder−order phase transition, the LSPR peak of the nanorods was blue-shifted from 712 to 614 nm (Figure 5D). This shift could be attributed to the decrease in aspect ratio during thermal treatment and/or the change of electronic structure due to phase transition.[55]

The disorder−order transition of individual Cu_3Au nanorods was further examined by *in situ* TEM equipped with a heating and cooling stage. No change of crystal structure was found by cooling from 25 °C (Figure 6A) to −262 °C (Figure 6D); that is, the nanorod remained disordered. Heating the sample from 25 °C to 327 °C (Figure 6B) transformed the disordered phase to the ordered phase. Further heating to 497 °C (Figure 6C) above the critical temperature (390 °C for the bulk)[56] reverted the ordered phase back to disordered phase, indicated by the disappearance of the (110) reflection spots. When the ordered phase was slowly cooled back to 25 °C, the nanorod underwent the phase transition through an equilibrium process and the well-ordered phase was kept uniformly at 25 °C (Figure 6E). On the other hand, when the disordered phase was rapidly cooled to 25 °C, the nanorod was preserved with short-range ordered structure, shown by the weak and diffusive (110) reflection spots in the ED pattern (Figure 6F). The disorder−order transformation was reversible, and either phase could be obtained repeatedly without significant alteration of the rod-shaped morphology; however, a decrease of aspect ratio was observed after heat treatment (Figure S4).

Intermetallic CuAu nanorods can also be synthesized by adjusting the mole ratio of Au to Cu precursors to 1:2 (Figure 7). All the peaks in the XRD pattern of the CuAu nanorods (17.7 ± 4.2 × 9.9 ± 1.9 nm) were indexed to the pattern expected for an ordered tetragonal CuAu phase.[53] Similar to the case of Cu_3Au, two sets of spots were observed in the ED pattern from an individual CuAu nanorod, one recorded from the [111] zone and the other viewed from the [110] zone, indicating that each CuAu nanorod was made of two single-crystal domains. An interface was clearly observed in the middle of the two domains as marked by arrows in the HRTEM. Based on the ED and FFT analyses, these CuAu nanorods were found to grow along the longitudinal ⟨110⟩ direction. The intermetallic CuAu nanorod could also be transformed from the disordered CuAu nanorods through heat treatment. In this case, the LSPR peak of the resultant nanorods was blue-shifted from 592 to 550 nm, indicating a decrease in aspect ratio during the annealing process.

This approach can be extended to other Cu-based bimetallic systems, for instance, Cu−Pt or Cu−Pd (Figure 8A,B). In either case, the Au seeds were replaced by Pt or Pd seeds, respectively, while all other conditions were kept identical to those for the Cu_3Au nanorod synthesis. XRD analysis confirmed the crystal structures and compositions were disordered Cu_3Pt and Cu_3Pd alloys, respectively (Figure 8C,D). The yield of elongated nanoparticles in both samples was around 50%. The relatively low yield could be attributed to the lower redox potential of $Pt(II)/Pt^0$ or $Pd(II)/Pd^0$ pairs relative to the $Au(I)/Au^0$ pair and the decreased lattice mismatch of Cu/Pt (7.9%) or Cu/Pd (7.8%) compared to Cu/Au (11%). Lowering the redox potential effectively slows the oxidation of Cu in the second step by reducing the loss of Cu^0 resulting from the galvanic replacement reaction; consequently, the reduction rate of Cu in the Cu−Pt or Cu−Pd system was faster than that in the Cu−Au system. A faster reduction rate favored production of core−shell particles over Janus particles during nucleation of Cu on the seeds. Switching to Ag nanoparticles as seeds, the overall rate of Cu reduction became faster because the remaining Ag(I) in the reaction could not effectively oxidize Cu^0. As a result, the product was predominated by Ag@Cu core−shell nanoparticles (Figure S5). Note that Cu is quickly oxidized to CuO in air, as indicated in the XRD analysis. As compared with Cu_3Au, the intensity of LSPR peaks in the visible region was significantly decreased for the Cu_3Pt and Cu_3Pd nanorods possibly due to the damping effect of the Pt and Pd metal in the alloys (Figure 8E,F).[57,58]

The catalytic activity of metallic nanoparticles is strongly correlated to their size, shape, and crystal structure. To evaluate the structure−activity relationship, different types of Cu_3Au bimetallic nanostructures were used to catalyze the reduction of

dx.doi.org/10.1021/jp4013653 | J. Phys. Chem. C 2013, 117, 8924−8932

p-nitrophenol by $NaBH_4$. Since this model reaction occurs in aqueous solution,[59] the Cu_3Au nanostructures were phase transferred to aqueous solution with the assistance of PEG-NH_2 before the catalytic measurement (Figure 9A). After PEGylation, there was little change to the morphology of the nanoparticles (Figure 9B). The discrepancy of the LSPR peak could be attributed to the difference in the refractive index of surface ligands and media.[60] For comparison, the concentration of Au atoms of each catalyst was held constant across catalytic measurements. When $NaBH_4$ is in excess, the reaction becomes a pseudo-first-order reaction for *p*-nitrophenol. The *p*-nitrophenol displays a strong absorbance peak at 400 nm in basic conditions (Figure S6), the decrease of which was monitored to obtain the apparent rate constant (k_{app}) of the reaction (Figure 9C,D). The k_{app} and the introduction time (t_0) for different catalysts are listed in Table 1. For both nanorods (NRs) and nanoparticles (NPs), the k_{app} of catalysts with ordered phase was almost twice as large as that of the catalysts with disordered phase. It is implied that the surface of Cu_3Au intermetallic nanostructures are more active than that of the disordered nanostructures. For the same crystal phase, the rod-shaped catalysts were close to twice as effective as spherical nanoparticle catalysts despite the 4-fold decrease in total surface area. The enhanced catalytic activity of Cu_3Au nanorods could be ascribed to the existence of high-index facets as compared to that of the nanospheres.[61,62] Note that the variation of t_0 was possibly due to the difference in surface ligand density and/or the structural reconstruction.[59]

CONCLUSION

The Cu-based alloyed nanorods have been successfully synthesized by controlling the reduction kinetics of a seeded co-reduction method. As demonstrated in Cu−Au system, the aspect ratio and composition of the alloyed nanorods could be controlled by adjusting the concentration of the Au seeds and altering the precursor ratio, respectively. The LSPR peak of the Cu_3Au nanorods could be readily tuned over the spectrum from visible to infrared. Additionally, the Cu_3Au nanostructures have demonstrated different catalytic activities for the reduction of *p*-nitrophenol in the order of ordered Cu_3Au nanorods > disordered Cu_3Au nanorods > ordered Cu_3Au nanoparticles > disordered Cu_3Au nanoparticles. The asymmetric seeded growth was extended to other Cu-based binary systems, specifically Cu−Pt and Cu−Pd. This method may represent a robust approach to produce a variety of binary, rod-shaped nanostructures with a broad range of tunable compositions and properties.

ASSOCIATED CONTENT

Supporting Information

Figures S1−S6. This material is available free of charge via the Internet at http://pubs.acs.org.

AUTHOR INFORMATION

Corresponding Author

*E-mail chenj@uark.edu; Ph +1 479-575-6203.

Notes

The authors declare no competing financial interest.

ACKNOWLEDGMENTS

This work was supported in part by the Ralph E. Powe Jr. Faculty Enhancement Award, funds from Arkansas Bioscience Institute, and startup funds from the University of Arkansas to J.C. The work at BNL was supported by the U.S. Department of Energy (Basic Energy Sciences) and by the Materials Science and Engineering Division under Contract DE-AC02-98CH10886 and through the use of CFN.

REFERENCES

(1) Ferrando, R.; Jellinek, J.; Johnston, R. L. Nanoalloys: From Theory to Applications of Alloy Clusters and Nanoparticles. *Chem. Rev.* **2008**, *108*, 845−910.

(2) Bracey, C. L.; Ellis, P. R.; Hutchings, G. J. Application of Copper-Gold Alloys in Catalysis: Current Status and Future Perspectives. *Chem. Soc. Rev.* **2009**, *38*, 2231−2243.

(3) Wang, D.; Li, Y. Bimetallic Nanocrystals: Liquid-Phase Synthesis and Catalytic Applications. *Adv. Mater.* **2011**, *23*, 1044−1060.

(4) Jana, N. R.; Gearheart, L.; Murphy, C. J. Seed-Mediated Growth Approach for Shape-Controlled Synthesis of Spheroidal and Rod-like Gold Nanoparticles Using a Surfactant Template. *Adv. Mater.* **2001**, *13*, 1389−1393.

(5) Nikoobakht, B.; El-Sayed, M. A. Preparation and Growth Mechanism of Gold Nanorods (NRs) Using Seed-Mediated Growth Method. *Chem. Mater.* **2003**, *15*, 1957−1962.

(6) Habas, S. E.; Lee, H.; Radmilovic, V.; Somorjai, G. A.; Yang, P. Shaping Binary Metal Nanocrystals through Epitaxial Seeded Growth. *Nat. Mater.* **2007**, *6*, 692−697.

(7) Seo, D.; Yoo, C. I.; Jung, J.; Song, H. Ag−Au−Ag Heterometallic Nanorods Formed through Directed Anisotropic Growth. *J. Am. Chem. Soc.* **2008**, *130*, 2940−2941.

(8) Lim, B.; Jiang, M.; Camargo, P. H. C.; Cho, E. C.; Tao, J.; Lu, X.; Zhu, Y.; Xia, Y. Pd-Pt Bimetallic Nanodendrites with High Activity for Oxygen Reduction. *Science* **2009**, *324*, 1302−1305.

(9) Peng, Z.; Yang, H. Synthesis and Oxygen Reduction Electrocatalytic Property of Pt-on-Pd Bimetallic Heteronanostructures. *J. Am. Chem. Soc.* **2009**, *131*, 7542−7543.

(10) Kobayashi, H.; Lim, B.; Wang, J.; Camargo, P. H. C.; Yu, T.; Kim, M. J.; Xia, Y. Seed-Mediated Synthesis of Pd−Rh Bimetallic Nanodendrites. *Chem. Phys. Lett.* **2010**, *494*, 249−254.

(11) Lim, B.; Kobayashi, H.; Yu, T.; Wang, J.; Kim, M. J.; Li, Z.-Y.; Rycenga, M.; Xia, Y. Synthesis of Pd−Au Bimetallic Nanocrystals via Controlled Overgrowth. *J. Am. Chem. Soc.* **2010**, *132*, 2506−2507.

(12) Ding, Y.; Fan, F.; Tian, Z.; Wang, Z. L. Atomic Structure of Au−Pd Bimetallic Alloyed Nanoparticles. *J. Am. Chem. Soc.* **2010**, *132*, 12480−12486.

(13) Xu, J.; Wilson, A. R.; Rathmell, A. R.; Howe, J.; Chi, M.; Wiley, B. J. Synthesis and Catalytic Properties of Au−Pd Nanoflowers. *ACS Nano* **2011**, *5*, 6119−6127.

(14) Wang, C.; Tian, W.; Ding, Y.; Ma, Y.-q.; Wang, Z. L.; Markovic, N. M.; Stamenkovic, V. R.; Daimon, H.; Sun, S. Rational Synthesis of Heterostructured Nanoparticles with Morphology Control. *J. Am. Chem. Soc.* **2010**, *132*, 6524−6529.

(15) Lu, C.-L.; Prasad, K. S.; Wu, H.-L.; Ho, J.-a. A.; Huang, M. H. Au Nanocube-Directed Fabrication of Au−Pd Core−Shell Nanocrystals with Tetrahexahedral, Concave Octahedral, and Octahedral Structures and Their Electrocatalytic Activity. *J. Am. Chem. Soc.* **2010**, *132*, 14546−14553.

(16) Yu, Y.; Zhang, Q.; Liu, B.; Lee, J. Y. Synthesis of Nanocrystals with Variable High-Index Pd Facets through the Controlled Heteroepitaxial Growth of Trisoctahedral Au Templates. *J. Am. Chem. Soc.* **2010**, *132*, 18258−18265.

(17) Yang, C.-W.; Chanda, K.; Lin, P.-H.; Wang, Y.-N.; Liao, C.-W.; Huang, M. H. Fabrication of Au−Pd Core−Shell Heterostructures with Systematic Shape Evolution Using Octahedral Nanocrystal Cores and Their Catalytic Activity. *J. Am. Chem. Soc.* **2011**, *133*, 19993−20000.

(18) DeSantis, C. J.; Peverly, A. A.; Peters, D. G.; Skrabalak, S. E. Octopods versus Concave Nanocrystals: Control of Morphology by Manipulating the Kinetics of Seeded Growth via Co-Reduction. *Nano Lett.* **2011**, *11*, 2164−2168.

(19) DeSantis, C. J.; Sue, A. C.; Bower, M. M.; Skrabalak, S. E. Seed-Mediated Co-reduction: A Versatile Route to Architecturally Controlled Bimetallic Nanostructures. *ACS Nano* **2012**, *6* (3), 2617−2628.
(20) DeSantis, C. J.; Skrabalak, S. E. Core Values: Elucidating the Role of Seed Structure in the Synthesis of Symmetrically Branched Nanocrystals. *J. Am. Chem. Soc.* **2012**, *135*, 10−13.
(21) Sun, S.; Murray, C. B.; Weller, D.; Folks, L.; Moser, A. Monodisperse FePt Nanoparticles and Ferromagnetic FePt Nanocrystal Superlattices. *Science* **2000**, *287*, 1989−1992.
(22) Grzelczak, M.; Rodríguez-González, B.; Pérez-Juste, J.; Liz-Marzán, L. M. Quasi-Epitaxial Growth of Ni Nanoshells on Au Nanorods. *Adv. Mater.* **2007**, *19*, 2262−2266.
(23) Chen, W.; Yu, R.; Li, L.; Wang, A.; Peng, Q.; Li, Y. A Seed-Based Diffusion Route to Monodisperse Intermetallic CuAu Nanocrystals. *Angew. Chem., Int. Ed.* **2010**, *49*, 2917−2921.
(24) Wang, D.; Li, Y. One-Pot Protocol for Au-Based Hybrid Magnetic Nanostructures via a Noble-Metal-Induced Reduction Process. *J. Am. Chem. Soc.* **2010**, *132*, 6280−6281.
(25) Niu, Z.; Wang, D.; Yu, R.; Peng, Q.; Li, Y. Highly Branched Pt-Ni Nanocrystals Enclosed by Stepped Surface for Methanol Oxidation. *Chem. Sci.* **2012**, *3*, 1925−1929.
(26) Rathmell, A. R.; Bergin, S. M.; Hua, Y.-L.; Li, Z.-Y.; Wiley, B. J. The Growth Mechanism of Copper Nanowires and Their Properties in Flexible, Transparent Conducting Films. *Adv. Mater.* **2010**, *22*, 3558−3563.
(27) Zhang, D.; Wang, R.; Wen, M.; Weng, D.; Cui, X.; Sun, J.; Li, H.; Lu, Y. Synthesis of Ultralong Copper Nanowires for High-Performance Transparent Electrodes. *J. Am. Chem. Soc.* **2012**, *134*, 14283−14286.
(28) Wang, H.; Tam, F.; Grady, N. K.; Halas, N. J. Cu Nanoshells: Effects of Interband Transitions on the Nanoparticle Plasmon Resonance. *J. Phys. Chem. B* **2005**, *109*, 18218−18222.
(29) Chan, G. H.; Zhao, J.; Hicks, E. M.; Schatz, G. C.; Van Duyne, R. P. Plasmonic Properties of Copper Nanoparticles Fabricated by Nanosphere Lithography. *Nano Lett.* **2007**, *7*, 1947−1952.
(30) Pan, D.; Cai, X.; Yalaz, C.; Senpan, A.; Omanakuttan, K.; Wickline, S. A.; Wang, L. V.; Lanza, G. M. Photoacoustic Sentinel Lymph Node Imaging with Self-Assembled Copper Neodecanoate Nanoparticles. *ACS Nano* **2012**, *6*, 1260−1267.
(31) Rodriguez, J. A.; Liu, P.; Hrbek, J.; Evans, J.; Pérez, M. Water Gas Shift Reaction on Cu and Au Nanoparticles Supported on CeO2(111) and ZnO(000$\bar{1}$): Intrinsic Activity and Importance of Support Interactions. *Angew. Chem., Int. Ed.* **2007**, *46*, 1329−1332.
(32) Li, C. W.; Kanan, M. W. CO_2 Reduction at Low Overpotential on Cu Electrodes Resulting from the Reduction of Thick Cu_2O Films. *J. Am. Chem. Soc.* **2012**, *134*, 7231−7234.
(33) Henkel, A.; Jakab, A.; Brunklaus, G.; Sönnichsen, C. Tuning Plasmonic Properties by Alloying Copper into Gold Nanorods. *J. Phys. Chem. C* **2009**, *113*, 2200−2204.
(34) Motl, N. E.; Ewusi-Annan, E.; Sines, I. T.; Jensen, L.; Schaak, R. E. Au−Cu Alloy Nanoparticles with Tunable Compositions and Plasmonic Properties: Experimental Determination of Composition and Correlation with Theory. *J. Phys. Chem. C* **2010**, *114*, 19263−19269.
(35) Xu, Z.; Lai, E.; Shao-Horn, Y.; Hamad-Schifferli, K. Compositional Dependence of the Stability of AuCu Alloy Nanoparticles. *Chem. Commun.* **2012**, *48*, 5626−5628.
(36) Sra, A. K.; Schaak, R. E. Synthesis of Atomically Ordered AuCu and $AuCu_3$ Nanocrystals from Bimetallic Nanoparticle Precursors. *J. Am. Chem. Soc.* **2004**, *126*, 6667−6672.
(37) Sra, A. K.; Ewers, T. D.; Schaak, R. E. Direct Solution Synthesis of Intermetallic AuCu and $AuCu_3$ Nanocrystals and Nanowire Networks. *Chem. Mater.* **2005**, *17*, 758−766.
(38) Liu, Q.; Yan, Z.; Henderson, N. L.; Bauer, J. C.; Goodman, D. W.; Batteas, J. D.; Schaak, R. E. Synthesis of CuPt Nanorod Catalysts with Tunable Lengths. *J. Am. Chem. Soc.* **2009**, *131*, 5720−5721.
(39) Xu, D.; Liu, Z.; Yang, H.; Liu, Q.; Zhang, J.; Fang, J.; Zou, S.; Sun, K. Solution-Based Evolution and Enhanced Methanol Oxidation Activity of Monodisperse Platinum−Copper Nanocubes. *Angew. Chem., Int. Ed.* **2009**, *48*, 4217−4221.
(40) Zhang, L.; Hou, F.; Tan, Y. Shape-Tailoring of CuPd Nanocrystals for Enhancement of Electro-catalytic Activity in Oxygen Reduction Reaction. *Chem. Commun.* **2012**, *48*, 7152−7154.
(41) Xu, Z.; Shen, C.; Hou, Y.; Gao, H.; Sun, S. Oleylamine as Both Reducing Agent and Stabilizer in a Facile Synthesis of Magnetite Nanoparticles. *Chem. Mater.* **2009**, *21*, 1778−1780.
(42) Ortiz, N.; Skrabalak, S. E. Manipulating Local Ligand Environments for the Controlled Nucleation of Metal Nanoparticles and Their Assembly into Nanodendrites. *Angew. Chem., Int. Ed.* **2012**, *51*, 11757−11761.
(43) Meffre, A.; Lachaize, S.; Gatel, C.; Respaud, M.; Chaudret, B. Use of Long Chain Amine as a Reducing Agent for the Synthesis of High Quality Monodisperse Iron(0) Nanoparticles. *J. Mater. Chem.* **2011**, *21*, 13464−13469.
(44) Jin, M.; Zhang, H.; Wang, J.; Zhong, X.; Lu, N.; Li, Z.; Xie, Z.; Kim, M. J.; Xia, Y. Copper Can Still Be Epitaxially Deposited on Palladium Nanocrystals To Generate Core−Shell Nanocubes Despite Their Large Lattice Mismatch. *ACS Nano* **2012**, *6*, 2566−2573.
(45) Langille, M. R.; Zhang, J.; Mirkin, C. A. Plasmon-Mediated Synthesis of Heterometallic Nanorods and Icosahedra. *Angew. Chem., Int. Ed.* **2011**, *50*, 3543−3547.
(46) Zeng, J.; Zhu, C.; Tao, J.; Jin, M.; Zhang, H.; Li, Z.-Y.; Zhu, Y.; Xia, Y. Controlling the Nucleation and Growth of Silver on Palladium Nanocubes by Manipulating the Reaction Kinetics. *Angew. Chem., Int. Ed.* **2012**, *51*, 2354−2358.
(47) Denton, A. R.; Ashcroft, N. W. Vegard's Law. *Phys. Rev. A* **1991**, *43*, 3161−3164.
(48) Mori, H.; Komatsu, M.; Takeda, K.; Fujita, H. Spontaneous Alloying of Copper into Gold Atom Clusters. *Philos. Mag. Lett.* **1991**, *63*, 173−178.
(49) Yasuda, H.; Mori, H.; Komatsu, M.; Takeda, K. Alloying Behavior of Gold Atoms into nm-Sized Copper Clusters. *Appl. Phys. Lett.* **1992**, *61*, 2173−2174.
(50) Yasuda, H.; Mori, H. Cluster-Size Dependence of Alloying Behavior in Gold Clusters. *Z. Phys. D: At., Mol. Clusters* **1994**, *31*, 131−134.
(51) Shibata, T.; Bunker, B. A.; Zhang, Z.; Meisel, D.; Vardeman, C. F.; Gezelter, J. D. Size-Dependent Spontaneous Alloying of Au−Ag Nanoparticles. *J. Am. Chem. Soc.* **2002**, *124*, 11989−11996.
(52) Liao, H.-G.; Cui, L.; Whitelam, S.; Zheng, H. Real-Time Imaging of Pt_3Fe Nanorod Growth in Solution. *Science* **2012**, *336*, 1011−1014.
(53) LaMer, V. K.; Dinegar, R. H. Theory, Production and Mechanism of Formation of Monodispersed Hydrosols. *J. Am. Chem. Soc.* **1950**, *72*, 4847−4854.
(54) Villars, P.; Calvert, L. D. *Pearson's Handbook of Crystallographic Data for Intermetallic Phases*, 2nd ed.; ASM International: Materials Park, OH, 1991.
(55) Skriver, H. L.; Lengkeek, H. P. Band Structure and Optical Properties of Ordered $AuCu_3$. *Phys. Rev. B* **1979**, *19*, 900−910.
(56) Hansen, M.; Anderko, K. *Constitution of Binary Alloys*; McGraw-Hill: New York, 1958.
(57) Schmidt, B. F.; Lynch, D. W. Optical Properties and Piezoreflectance of Silver-Palladium Alloys. *Phys. Rev. B* **1971**, *3*, 4015−4023.
(58) Myers, H. P.; Walldén, L.; Karlsson, Å. Some optical properties of CuPd, AgPd, AuPd and CuMn, AgMn alloys. *Philos. Mag.* **1968**, *18*, 725−744.
(59) Herves, P.; Perez-Lorenzo, M.; Liz-Marzan, L. M.; Dzubiella, J.; Lu, Y.; Ballauff, M. Catalysis by Metallic Nanoparticles in Aqueous Solution: Model Reactions. *Chem. Soc. Rev.* **2012**, *41*, 5577−5587.
(60) Willets, K. A.; Van Duyne, R. P. Localized Surface Plasmon Resonance Spectroscopy and Sensing. *Annu. Rev. Phys. Chem.* **2007**, *58*, 267−297.
(61) Carbó-Argibay, E.; Rodríguez-González, B.; Gómez-Graña, S.; Guerrero-Martínez, A.; Pastoriza-Santos, I.; Pérez-Juste, J.; Liz-Marzán, L. M. The Crystalline Structure of Gold Nanorods Revisited: Evidence

for Higher-Index Lateral Facets. *Angew. Chem., Int. Ed.* **2010**, *49*, 9397−9400.
(62) Wang, Z. L.; Gao, R. P.; Nikoobakht, B.; El-Sayed, M. A. Surface Reconstruction of the Unstable {110} Surface in Gold Nanorods. *J. Phys. Chem. B* **2000**, *104*, 5417−5420.